The Journal of Green Energy and Environmental Engineering

Research Paper

# Corncob Prepared Bonded Dust Suppression Materials with the Performance Analysis

**Phisit Matsumnra[1], Bahman Khalafi[2,*]**

[1] NTT Hi-Tech Institute, Nguyen Tat Thanh University, 298-300A Nguyen Tat Thanh, District 4, Ho Chi Minh City 755414, Vietnam

[2] Laboratório de Materiais Magnéticos Nanoestruturados, LaMMaN, Programa de Pós-Graduação em Nanociências, Universidade Franciscana-UFN, Santa Maria, RS, 97010-032, Brazil

*Corresponding author: Bahm.Khalafi@gmail.com

**Abstract.** To mitigate coal dust contamination jeopardizing railway operational safety attributed to suboptimal efficacy of conventional dust suppression agents, this investigation formulated an eco-friendly bio-derived adhesive particulate suppressant. Using corncob agricultural waste as the primary substrate, combined with acrylic acid monomer, ethylene glycol dimethacrylate as the crosslinker, and sodium dodecyl sulfate as the surfactant, a corncob-based dust suppression material was prepared. Comprehensive mechanistic investigation of tetracycline sorption onto porous biochar derived from peanut shells (PFBC) revealed multiple uptake pathways encompassing pore filling, π–π stacking interactions, hydrogen bonding, and metal complexation. Post-modification characterization indicated substantial enhancement of porosity, and surface oxygen-containing functional groups, with nanometer-scale particle dimensions. Sorption isotherm analysis confirmed Langmuir behavior with pseudo-second-order kinetic modeling, indicating monolayer chemisorption as the rate-limiting mechanism, achieving maximum sorption capacity of 500.0 mg/g at 25°C. The particulate suppression agent exhibited cohesive structural properties, forming a compact, flaky solidified stratum at the coal dust interface, thereby effectively sealing interstitial voids among particulate matter. The particulate suppression agent exhibited cohesive structural properties, forming a compact, flaky solidified stratum at the coal dust interface, thereby effectively sealing interstitial voids among particulate matter. Dynamic wetting characteristics of material molecules at the coal-water interface were revealed, comprising rapid molecular diffusion in early stages, oriented aggregation followed by cross-linked network development during intermediate phases, and final equilibration attained at 300 picoseconds. The unique bifunctional molecular configuration of the agent markedly augmented microscopic interfacial interactions between coal and aqueous molecules. Under these specified conditions, particulate peak Concentration reached 3.0 mg/m³ with asymptotic stabilization at 1.0 mg/m³. Comprehensive mechanistic investigation of tetracycline sorption onto porous biochar derived from peanut shells (PFBC) revealed multiple uptake pathways encompassing pore filling, π–π stacking interactions, hydrogen bonding, and metal complexation. Post-modification characterization indicated substantial enhancement of specific surface area, pore volume, and surface oxygen-containing functional groups, with nanometer-scale particle dimensions. Sorption isotherm analysis confirmed Langmuir behavior with pseudo-second-order kinetic modeling, indicating monolayer chemisorption as the rate-limiting mechanism, achieving maximum sorption capacity of 500.0 mg/g at 25°C. The unique dual-affinity molecular configuration of the agent markedly augmented microscopic interfacial interactions between coal and aqueous molecules. Experimental investigations utilizing a simulation experimental system established the optimal application concentration at 1.5% mass fraction. Under these specified conditions, particulate peak concentration reached 3.0 mg/m³ with asymptotic stabilization at 1.0 mg/m³. The temporal duration of particulate generation resulting from aerodynamic perturbation was 46 seconds, yielding optimal comprehensive dust suppression efficacy.

**Keywords:** *Coal transportation; Adhesive materials; Micro performance; Dust suppression mechanism; Corncob; Molecular dynamics simulation; Simulation experiment*

Received on 15 Feb 2025, Accepted on 15 April 2025, Published on 15 May 2025



## 1 Introduction

Coal serves as a critical and irreplaceable energy resource within China's energy portfolio. Coal serves as a

critical and irreplaceable energy resource within China's energy portfolio, with its extraction and logistics playing a pivotal role in sustaining national economic growth. Rail transit constitutes the predominant modality for coal distribution, representing in excess of 70% of the aggregate shipping volume [1-3].During railway transit of coal through tunnel infrastructure, aerodynamic interactions between high-velocity airflow and exposed coal surfaces generate particulate matter, thereby compromising both environmental quality within the tunnel and operational safety of rail transport [4-6].

In recent years, chemical dust suppression agents have found extensive application across diverse phases of coal extraction operations,transfer, and logistics. Researchers globally have conducted comprehensive investigations into coal dust suppression technologies, yielding significant advancements. Cheng Shuyan and colleagues [7] utilized waste paper as the feedstock material, whereas extracted and refined cellulose to synthesize carboxymethyl cellulose, demonstrating favorable efficacy in particulate matter suppression. Luo Ruidong and colleagues [8] engineered a particulate-inhibiting formulation utilizing isolated soy protein as the foundational matrix, subsequently incorporating sodium dodecyl sulfonate and carboxymethyl cellulose sodium salt as auxiliary constituents to enhance overall efficacy. Additionally, sodium methyl silicate was integrated into the formulation, capable of generating a solidified crust upon the coal dust surface to facilitate solidification.

Ma et al. [9] used graft copolymerization technology to prepare a polymeric dust suppression material and compounded it with surfactants, achieving relatively ideal dust suppression effects. Nie Wen et al. [10-11] introduced polydopamine into an acrylamide polymerization reaction system at low temperatures to generate a dust suppression material, which, when compounded with surfactants and hygroscopic inorganic salts, could effectively suppress dust. Zhou Gang et al. [12-13] used cedar sawdust as raw material to obtain delignified wood powder and prepared a new type of green, highly water-absorbent dust suppression material via microwave-assisted in-situ synthesis. The aforementioned results have effectively reduced coal dust pollution in various production stages. However, existing dust suppression materials are susceptible to secondary environmental contamination or involve substantial production expenses, However, existing dust suppression materials are susceptible to secondary environmental contamination or involve substantial production expenses,

Corncob, as an agricultural waste, has become an ideal dust suppression material due to its renewability and environmental friendliness. The intrinsic cellulose framework and porous architecture of corncob confer exceptional moisture retention and adhesion characteristics, surpassing those of conventional inorganic dust suppression agents; its chemical composition, primarily comprising cellulose, hemicellulose, and lignin, facilitates complete environmental degradation, thereby circumventing the persistent contamination issues inherent to conventional dust suppression methodologies [14-17].Furthermore, the valorization of corncob waste mitigates environmental burdens associated with traditional disposal practices, such as open-air burning. Consequently, this investigation employs corncob as the foundational substrate for the development of a bio-based bonded dust suppression formulation, establishes the optimal reagent proportion and elucidates the underlying particulate suppression mechanism at the microscopic scale, and determines the optimal spraying concentration, thereby establishing a foundational basis for coal transportation dust pollution prevention and control strategies.

## 2 Materials and Methods

### 2.1 Material Preparation

The corncob substrate was comminuted and sieved through a 100-mesh aperture to achieve particle size uniformity. Precisely measure 1.5 g of the prepared specimen and introduce it into a 500 mL reaction vessel. Add 300 mL of PW and mix thoroughly at a stirring speed of 60 r/min. Subsequently, introduce the chain transfer agent SBS solution,elevate the system temperature to 60°C, while maintaining isothermal conditions. Gradually introduce 3 mL of 25% mass fraction AA solution and 1 mL of 10% mass fraction initiator APS solution via dropwise addition, respectively. Allow the reaction to proceed for 2 hours. Following reaction completion, sequentially introduce 5 mL of 30% mass fraction neutralizing agent SH solution and 3 mL of crosslinker EGDMA solution. Ultimately, introduce 3 mL of SDS surfactant solution and 3 mL of AS humectant solution, maintaining agitation at 60 r/min for an additional hour to yield the experimental formulation.The preparatory workflow is

schematically depicted in Figure 1.

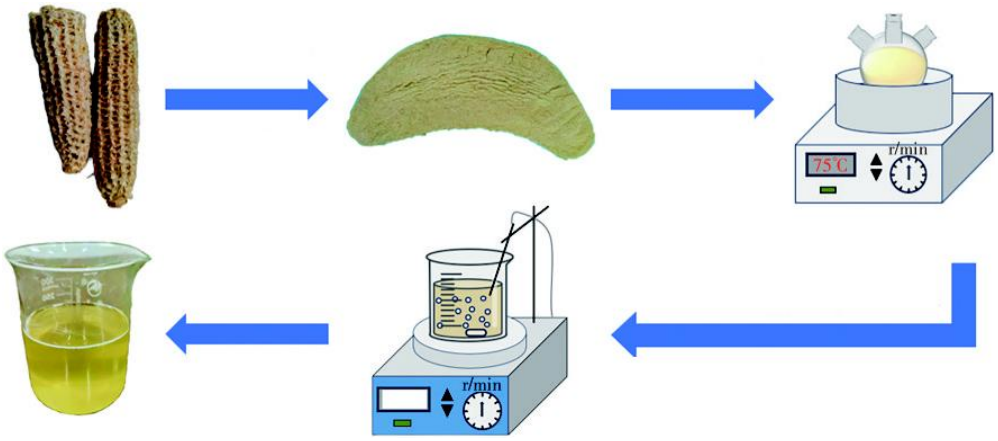


**Figure 1** Figure 1 Preparation process of dust suppression material

During this procedure, acrylic acid undergoes neutralization with sodium hydroxide to generate sodium acrylate.In the presence of initiator APS and chain transfer agent SBS,molecular chain scission and subsequent polymerization occur, yielding sodium polyacrylate (PAAS). molecular chain scission and subsequent polymerization occur, yielding sodium polyacrylate (PAAS). forming a superabsorbent resin. The incorporation of surfactant SDS and humectant AS yields the final experimental formulation.

### 2.2 Coal Sample Preparation

The bituminous coal specimen employed in experimentation was classified as Shenhun No. 1 variety, sourced from railway spillage incidents occurring within the Liangjiashan Tunnel.Proximate analysis of the coal specimen, normalized to air-dried conditions, indicated moisture content at 1.7%, ash yield of 12%, volatile matter fraction of 21%, and total sulfur concentration of 0.6%. Prior to experimental procedures, the coal specimen underwent thermal conditioning at 105°C until mass stabilization was achieved, subsequently comminuted and sieved via 60-mesh aperture to ensure particle size uniformity. Granulometric characterization was performed employing a Winner 2309 laser diffraction instrument to ascertain the particle size distribution of the dust specimen. The particle size parameters are as follows: small particle size 4.12 μm, median particle size 22.34 μm, large particle size 78.25 μm.

## 3 Optimization of Material Ratio

### 3.1 Material Ratio Scheme

Acrylic acid (AA), serving as the monomeric precursor, contributes the highly hydrophilic polymer constituent. Ethylene glycol dimethacrylate (EGDMA) functions as the cross-linking agent, thereby augmenting the structural integrity of the resultant material. Sodium dodecyl sulfate (SDS) enhances material wettability via its surfactant-mediated interfacial activity. Preliminary experimental findings demonstrated that elevated proportions of either acrylic acid (AA) or sodium dodecyl sulfate (SDS) compromise material performance resulting in either excessive reagent viscosity or pronounced emulsification effects. Conversely, diminished proportions of these constituents result in inadequate cellulose grafting efficiency or suboptimal wetting characteristics, thereby compromising experimental reproducibility. This observation is consistent with the empirical findings documented by Jin et al. Studies [18-20] on superabsorbent resin fabrication employing corn stalk fiber and acrylic acid as precursor materials further corroborate the pivotal importance of stoichiometric proportions in the graft polymerization process. Consequently, to mitigate experimental anomalies attributable to univariate parameter deviations, an orthogonal experimental design was implemented in this investigation. The precise reagent proportions were as follows: AA: EGDMA: SDS of 1:1:1, 2:1:1, 1:1:2, 1:2:1, and 2:1:2, resulting in Materials I~VII.

### 3.2 Environmental Stability Testing of Dust Suppression Material

### 3.2.1 Anti-evaporation Test

Anti-evaporation assessments were performed on identical quantities of deionized water and Experimental Materials I through VII under controlled thermal conditions maintained at 40°C, 60°C, and 80°C. Specimens were subjected to gravimetric evaluation at 2-hour intervals utilizing a precision analytical balance, with sustained monitoring maintained throughout a 12-hour observation period.

The anti-evaporation property of the material is characterized by the evaporation rate [21-22], as shown in Equation (1).

$$\theta=(m1-m2)/AT \quad (1)$$

Where, θis the material evaporation rate, g/(m²·s); m1 is the material mass before evaporation, g; m2 is the material mass after evaporation, g; A is the container bottom area, m²; T is the evaporation time, s.

### 3.2.2 Crust Solidification Test

Under isothermal conditions maintained at 25°C, Experimental Materials I through VII were uniformly applied to coal dust specimen surfaces via atomization at a deposition density of 2.5 L/m².Surface crust microstructure, temporal evolution of crust development, and crustal thickness measurements were systematically documented at 0.5-hour intervals for each specimen.

### 3.2.3 Wind Erosion Resistance Test

Equivalent quantities of pure water and Experimental Materials I–VII were sprayed onto coal dust specimens and exposed to outdoor atmospheric conditions for wind erosion assessment. Specimens underwent gravimetric analysis at 2-hour intervals using a high-precision analytical balance, with uninterrupted monitoring extended over a 24-hour timeframe.

Aerodynamic degradation resistance of the material was quantified through wind erosion rate parameters [23-24], as mathematically delineated in Equation (2).

$$E=(m0-m)/m0\times100\% \quad (2)$$

Where, E is the wind erosion rate, %; m0 is the coal dust mass before erosion, g; m is the coal dust mass after erosion, g.

### 3.3 Test Results

### 3.3.1 Material Anti-evaporation Property

The evaporation rate (θ) determination outcomes for the experimental formulations under controlled thermal conditions of 40°C, 60°C, and 80°C are illustrated in Figure 2. Analysis of Figure 2 reveals that the evaporation rate (θ) progression can be delineated into three distinct stages: Characterized by intensified internal molecular thermal motion and elevated surface water molecular kinetic energy,Characterized by progressive hydration film formation on the material surface, thereby inhibiting water molecule escape, resulting in gradual θ reduction. Characterized by stabilization of the surface hydration film structure, with θ approaching equilibrium.

Under varying thermal conditions, Experimental Materials I–VII demonstrate significantly reduced evaporation rates compared to pure water, thereby evidencing superior moisture retention characteristics.At an experimental temperature of 40°C, the mean evaporation rates (θ) for Materials I, V, VI, and VII remain below 0.02 g/(m²·s), with Material VI exhibiting the minimum average θ of 0.0153 g/(m²·s), whereas other formulations demonstrate mean θ values exceeding 0.03 g/(m²·s). At 60°C, the mean Evaporation Rates (θ) for Materials I, III, IV, and VI remain below 0.07 g/(m²·s), with Material IV demonstrating the minimum average θ of 0.0337 g/(m²·s), whereas other formulations exhibit mean θ values exceeding 0.08 g/(m²·s). At 60°C, the mean Evaporation Rates (θ) adhere to the following hierarchy: Material IV < Material III < Material I < Material VI < Material II < Material VII. At 80°C, the mean Evaporation Rates (θ) for Materials I and VI remain below 0.08 g/(m²·s), with Material VI exhibiting the minimum average θ of 0.0742 g/(m²·s), whereas other formulations demonstrate mean θ values approaching 0.1 g/(m²·s)At 80°C, the mean Evaporation Rates (θ) follow the sequence: Material VI < Material I <

Material IV < Material III < Material II < Material VII < Material V. Comparative assessment reveals that Experimental Materials I and VI demonstrate superior moisture retention properties and enhanced thermal stability compared to alternative formulations.

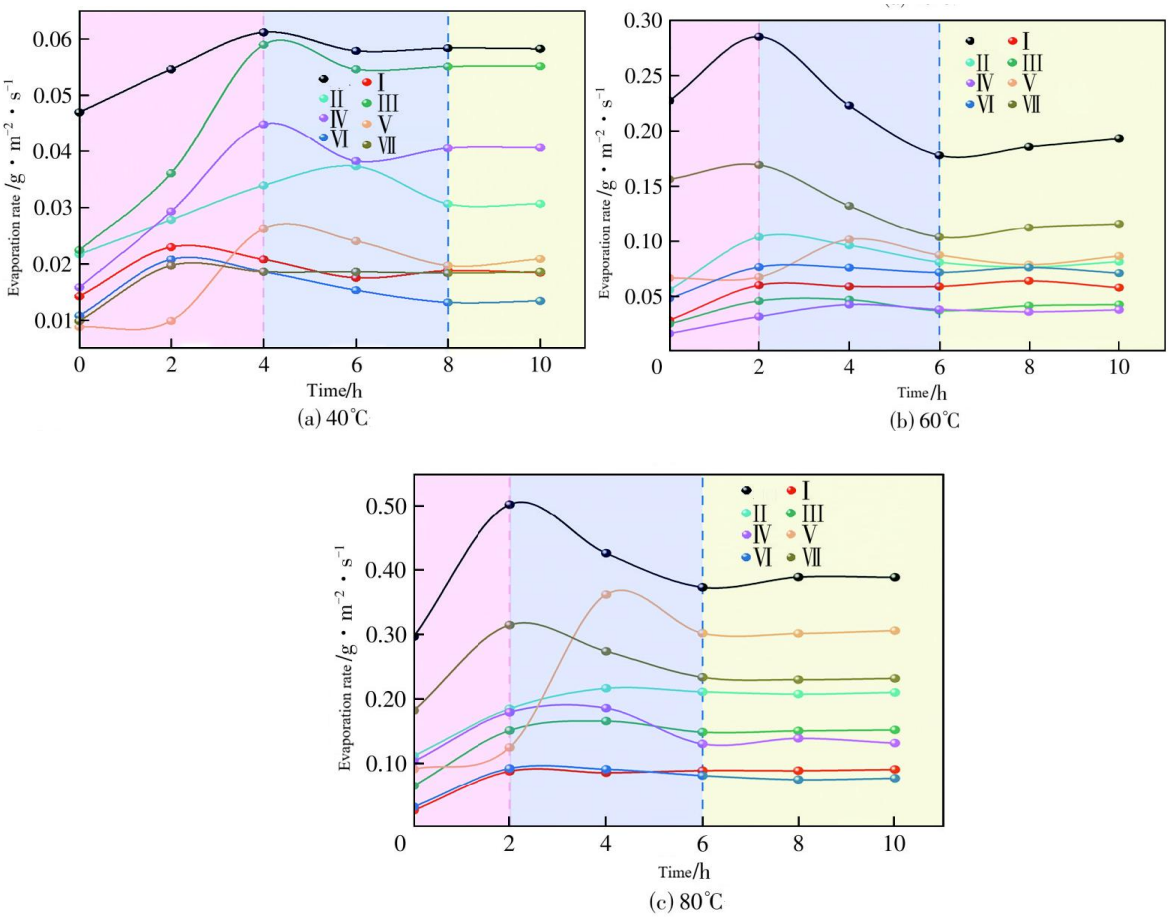


**Figure 2** Evaporation rate of experimental materials at different temperatures

### 3.3.2 Material Crust Solidification

Figure 3 shows the solidification and crusting results of Experimental Materials I~VII, and Figure 4 shows the material solidification time and crust thickness.

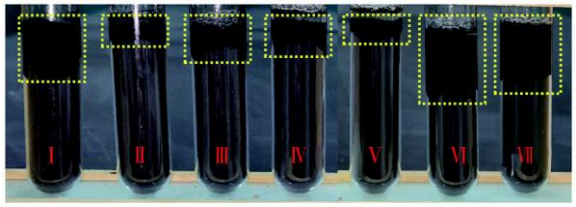


**Figure 3** The solidification structure of the experimental material

From Figures 3 and 4, it can be seen that the solidification times of Materials I~VII are 5 h, 5.5 h, 4 h, 6 h, 7 h, 4.5 h, and 6.5 h, respectively, satisfying: Material III < Material VI < Material I < Material II < Material IV < Material VII < Material V. The crust thicknesses of Materials I~VII are 2 cm, 0.7 cm, 1.4 cm, 1.3 cm, 0.6 cm, 3.1 cm, and 2.6 cm, respectively, satisfying: Material V < Material II < Material IV < Material III < Material I < Material VII < Material VI. Comparative assessment revealed that Experimental Materials I and VI demonstrated abbreviated solidification intervals and enhanced crust thickness relative to alternative formulations.

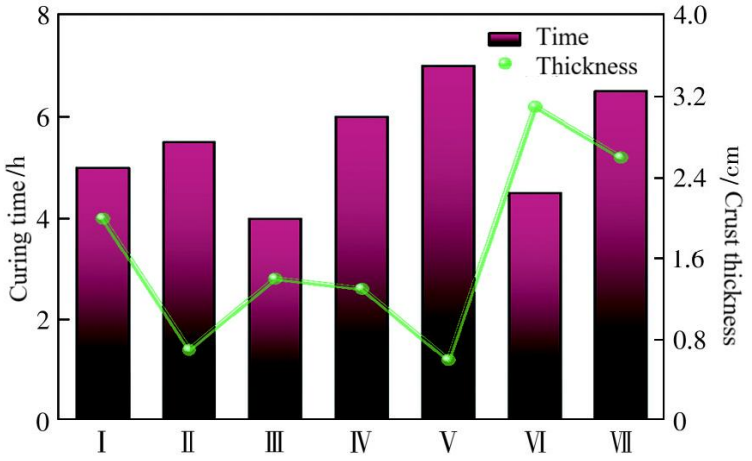


**Figure 4** Experimental material solidification time and crust thickness

### 3.3.3 Material Wind Erosion Resistance

This investigation quantified coal dust mass loss throughout the wind erosion experimental stages, with results presented in Figure 5. The aerodynamic degradation resistance, quantified as Wind Erosion Rate (E), was further computed for coal dust specimens treated with diverse dust suppression formulations, with resultant data compiled in Table 1.

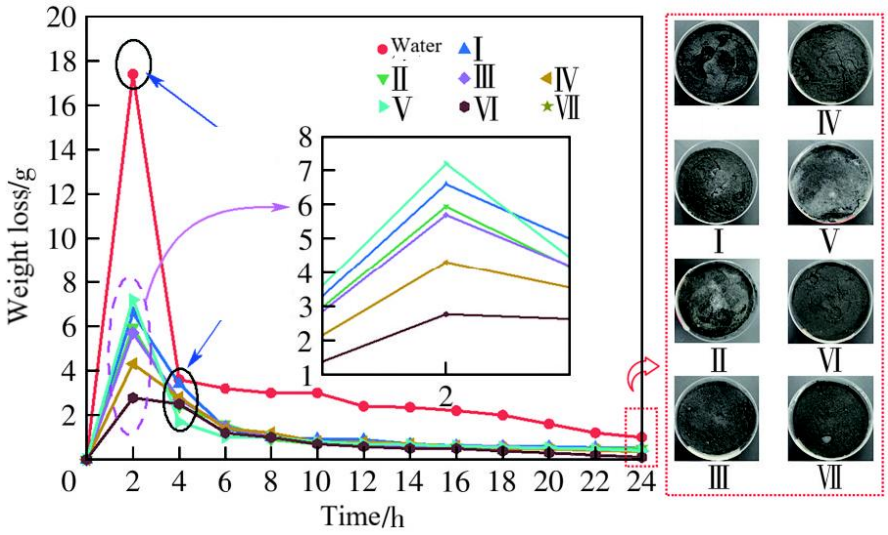


**Figure 5** Coal Dust Loss Quality

Analysis of Figure 5 reveals that Coal Dust Mass Loss for specimens treated with pure water and Experimental Materials I–VII exhibits an initial increase, subsequent decrease, and ultimate stabilization over the experimental duration.During the 0–2 hour interval, incomplete material penetration renders Coal Dust susceptible to wind force, resulting in rapid mass loss escalation to peak values. The minimal Coal Dust Mass Loss, quantified at 2.8 g, was observed for specimens treated with Experimental Material VI.During the 2–4 hour interval, material infiltration into Coal Dust interior occurs, accompanied by progressive solidification and crust formation, resulting in rapid mass loss reduction. At 80°C, the mean Evaporation Rates (θ) follow the sequence: Material VI < Material I < Material IV < Material III < Material II < Material VII < Material V. Comparative assessment reveals that Experimental Materials I and VI demonstrate superior moisture retention properties and enhanced thermal stability compared to alternative formulations. Following the 4-hour mark, material solidification and crusting phenomena stabilize,resulting in Coal Dust Mass Loss values below 1 g for

all experimental formulations. Notably, specimens treated with Experimental Material VI consistently demonstrate the minimal mass loss.

It was analyzed that Pure Water application yields a Wind Erosion Rate (E) of 69% for Coal specimens. Material I~VII showed a E value of 26^, 24%, 25%, 26%, 25%, 18%, and 23%. Following application of experimental formulations, the Wind Erosion Rate (E) undergoes substantial reduction, averaging 45.1% decrease. Among Experimental Materials I–VII, Materials I and IV exhibit the maximum Wind Erosion Rate (E) at 26%, whereas Material VI demonstrates the minimum E at 18%.

## 4 Micro-Performance Characterization of Dust Suppression Material

### 4.1 Scanning Electron Microscopy (SEM)

The CBS-PAAS formulation was subjected to thermal conditioning at 60°C until mass stabilization, followed by comminution and sieving through a 100-mesh aperture, prior to Scanning Electron Microscopy (SEM) examination.The Scanning Electron Microscopy (SEM) characterization outcomes for Corncob (CC) powder, CBS-PAAS powder, and Coal Dust following CBS-PAAS treatment are depicted in Figure 6.

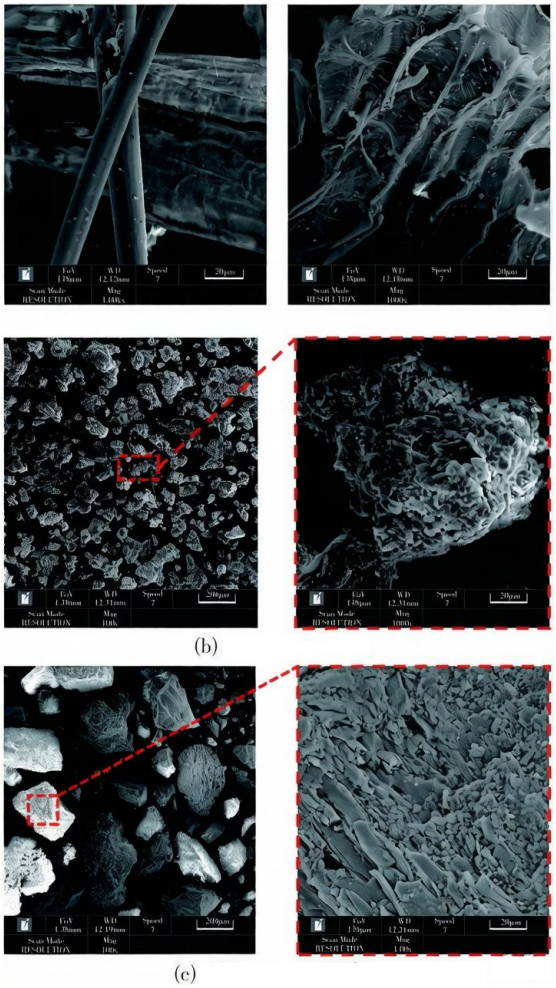


**Figure 6** Scanning Electron Microscope Experimental Results

As depicted in Figure 6(a), Corncob (CC) exhibits abundant lignin, Cellulose, and Hemicellulose constituents. The molecular architecture of Lignin encompasses diverse reactive moieties, including aromatic functionalities, phenolic hydroxyl substituents, alcoholic hydroxyl groups, and carbonyl-conjugated unsaturated bonds; Cellulose is characterized by abundant polar functional groups, notably hydroxyl and carboxyl moieties. These structural

characteristics enable lignin and cellulose to provide a large number of strong hydrophilic groups, laying the molecular foundation for the graft copolymerization reaction, biodegradability, and enhancement of hydrophilicity of the dust suppression material. The hemicellulose in corncob swells after water absorption, and its microstructure gradually expands and flattens from its initial curled state, further enhancing its interaction ability with water molecules.

As shown in Figure 6(b), CBS-PAAS exhibits a bonded structure, with obvious agglomeration occurring between particles. Fine particulates undergo agglomeration through interparticle interactions, thereby demonstrating the robust cohesive properties of CBS-PAAS. Under elevated magnification, the CBS-PAAS surface exhibits fine, lamellar morphological features, which facilitate adsorption onto larger agglomerate surfaces through van der Waals interactions. Additionally, these lamellar structures demonstrate rapid aqueous dissolution kinetics, thereby circumventing dissolution incompleteness attributable to insufficient thermal or mechanical agitation.

As illustrated in Figure 6(c), CBS-PAAS induces Coal Dust particle adhesion and agglomeration, thereby reducing particulate dispersion; furthermore, CBS-PAAS occupies interstitial voids between Coal Dust particles, thereby enhancing structural stability.Under elevated magnification, CBS-PAAS forms a homogeneous, dense, Lamellar Solidified Layer on Coal Dust particle surfaces. These structural features collectively enhance interparticle cohesive forces and effectively suppress dust liberation phenomena.

**4.2 Infrared Spectroscopy Experiment**

Fourier Transform Infrared (FTIR) Spectroscopy serves as a critical analytical technique for investigating functional group transformations and reaction mechanism elucidation. Fourier-transform infrared spectroscopic analysis of CC-CBS-PAAS composite materials is presented in Figure 7.From Figure 7(a), for CC, the characteristic peak appearing at 3421 $cm^{-1}$ is attributed to the stretching vibration of -OH, indicating the presence of hydroxyl functional groups in the sample. The spectral feature observed at 2832 $cm^{-1}$ is attributable to C-H stretching vibrations of methylene ($-CH_2-$) moieties within cellulose, while the absorption maximum at 2717 $cm^{-1}$ originates from C-H stretching modes associated with the lignin aromatic framework.The distinctive absorption band at 1623 $cm^{-1}$ is assignable to C=C stretching vibrations within the aromatic lignin framework, thereby confirming the structural presence of lignin.

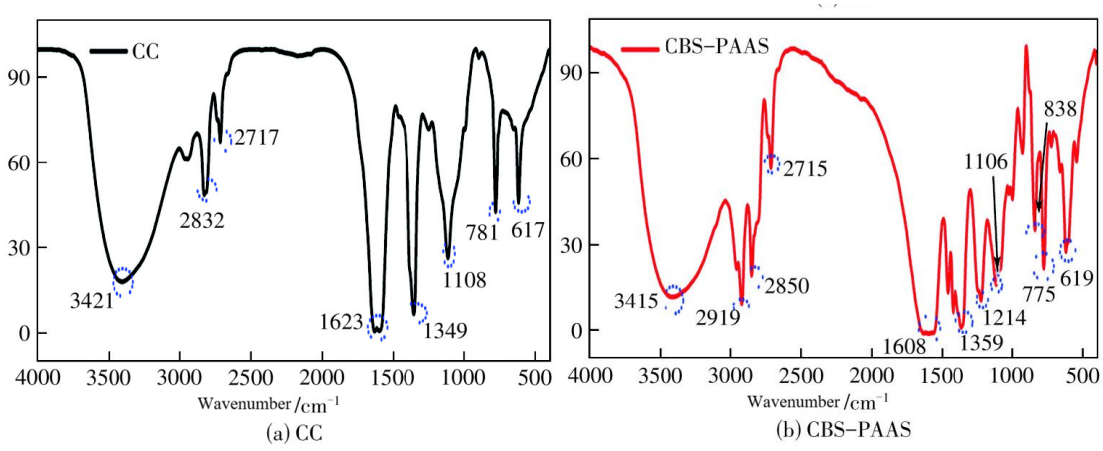


**Figure 7** Experimental results of CC and CBS-PAAS infrared spectra

Furthermore, the absorption feature at 1349 $cm^{-1}$ is attributable to asymmetric C-O-C stretching modes bridging sugar ring structures within cellulose and hemicellulose.The appearance of these distinctive absorption bands corroborates the existence of cellulose, hemicellulose, and lignin components within the corncob (CC) matrix. Examination of Figure 7(b) demonstrates that CBS-PAAS preserves the hydroxyl (-OH) stretching vibration at 3415 $cm^{-1}$ while displaying carbon-carbon double bond stretching at 1608 $cm^{-1}$, thereby retaining select structural attributes of the native corncob (CC) framework.

Additionally, the C-H stretching vibration observed at 2919 $cm^{-1}$ can be attributed to Alkyl Chain structures

formed through the the reaction between Sodium Dodecyl Sulfate (SDS) and Acrylic Acid (AA). The absorption band at 1214 $cm^{-1}$ is assignable to C-O stretching vibrations, thereby substantiating the occurrence of free radical cross-linking reactions between the crosslinking agent ethylene glycol dimethacrylate (EGDMA) and the constituent components. The aforementioned results substantiate the successful occurrence of chemical reactions among reactants, thereby confirming the synthesis of the target dust suppression material with the intended structural configuration.

**5 Microscopic Dust Suppression Mechanism**

Computational simulations utilizing Materials Studio software were employed to model the migration behavior of the dust suppression material and its dynamic wetting characteristics on Coal Dust surfaces, as illustrated in Figure 8.The coal molecular model used for the simulation was optimized by introducing N elements based on the Wender model. The simulation was conducted under the Compass force field, and simulation trajectory data of 300 ps were selected for dynamic characteristic analysis. Given the distinctive Three-Dimensional structural characteristics of the dust suppression material, the computational model constructed for simulation purposes oriented the dust suppression material molecules perpendicular to the Coal surface, specifically at the Coal-Water interface.

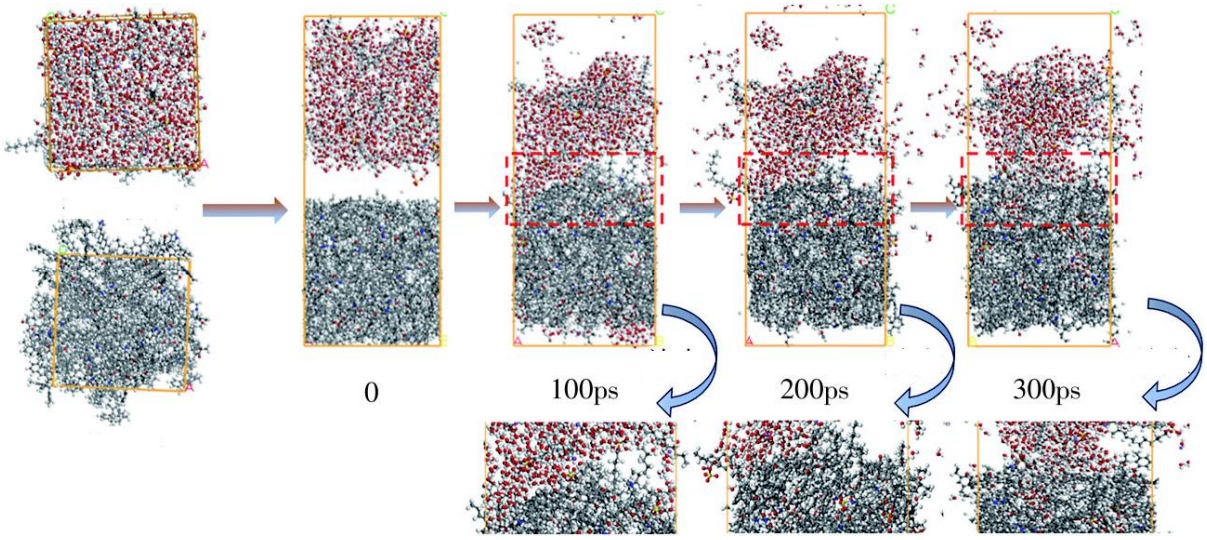


**Figure 8** Mechanism of Coal Dust, Water and CBS-PAAS

This orientation strategy circumvents the technical challenges associated with determining suppressant end-group orientations in conventional planar deposition methods, while simultaneously enhancing computational efficiency regarding chemical reaction simulations [25-28].From Figure 8, in the initial state, the dust suppression material molecules and water molecules are distributed discretely. As temporal progression of the simulation advanced, terminal functional moieties of the dust suppression agent molecules exhibited preferential orientation and directional aggregation toward the coal matrix interface.Consequently, a cross-linked network architecture emerged via intermolecular interaction mechanisms. Following the establishment of diffusive equilibrium at 300 picoseconds, water molecules exhibited pronounced surface mobility across the coal substrate. Subsequent to equilibration at 300 ps, partial migration of both aqueous species and dust suppression agent molecules into microporous structures of the coal matrix was observed. This phenomenon enhances the interfacial contact area between Coal and Water phases.

To further elucidate the diffusion characteristics of Water and CBS-PAAS molecules on Coal Dust surfaces, the temporal evolution of Mean Square Displacement (MSD) for each molecular species was analyzed, as depicted in Figure 9. From Figure 9, it was found that drawing upon the aforementioned functional correlation between mean squared displacement (MSD) and temporal variable t, the temporal derivatives of $MSD_1$ and $MSD_2$ were determined to be 0.586 and 0.271, respectively. The computed diffusion coefficients for aqueous species ($D_1$ = 0.0976) and CBS-PAAS ($D_2$ = 0.0451) demonstrate that CBS-PAAS possesses enhanced adsorptive affinity toward

the coal dust interface, consequently establishing a stable molecular coating layer. This adsorbed stratum effectively obstructs aqueous molecule migration from the coal interface toward the external environment, thereby prolonging the persistence of surface moisture. In conclusion, hydrophobic functional moieties within the dust suppression agent molecules form stable chemisorptive bonds with coal surface functional groups, while hydrophilic segments promote aqueous molecule infiltration into the coal matrix via hydrogen bonding interactions. This distinctive dual-Affinity Molecular Architecture substantially enhances interfacial interactions between Water and Coal molecules at the microscopic scale.

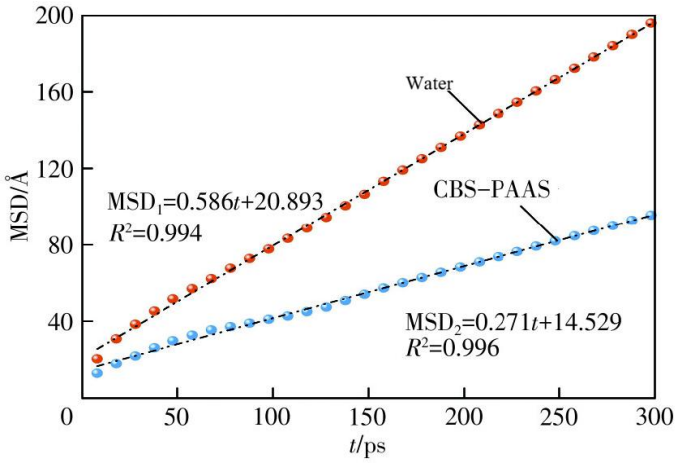


**Figure 9** Mean Square Displacement Situation

**6 Dust Suppression by CBS-PAAS**

The spraying concentration of the dust suppression material represents a critical parameter governing its efficacy in particulate matter suppression. A computational simulation framework was established to evaluate the dust suppression efficiency of CBS-PAAS across varying concentration regimes. As depicted in Figure 10, the experimental apparatus encompasses four integrated subsystems: a tunnel prototype, a railway vehicle model, a propulsion mechanism, and a monitoring array.The tunnel prototype measures 2.10 meter in length, 0.85 meter in height, and 0.76 meter in width. The railway vehicle model functions as the coal specimen carrier. The propulsion mechanism incorporates a single 4 kW 4-72-4A centrifugal blower, paired with two 1.5 kW 4-72-3.2A centrifugal blowers, alongside an integrated control cabinet. Anemometric sensors are deployed superior to the anterior, medial, and posterior segments of the railway vehicle model, while the particulate concentration detector is situated superior to the posterior segment of the railway vehicle model. Data streams from individual sensors are transmitted and processed instantaneously via the Data Acquisition and Processing Platform.

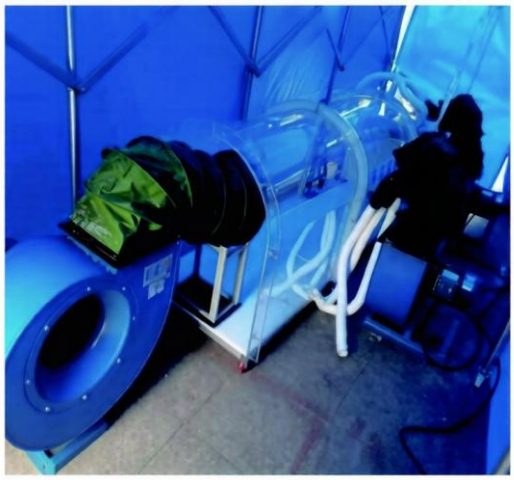

**Figure 10** Simulation Experiment System

Preliminary rheological characterization of CBS-PAAS across varying concentration regimes revealed that upon exceeding a 2% mass fraction threshold, solution viscosity increased markedly, thereby precluding effective atomization onto the coal specimen surface.Drawing upon these observations, four mass fraction conditions (0.5%, 1.0%, 1.5%, and 2.0%) were designated for experimental evaluation, with untreated coal specimens and those treated solely with deionized water serving as control groups. The aerodynamic perturbation induced by railway vehicle transit through tunnel infrastructure can reach velocities approaching 10 m/s; accordingly, the experimental wind velocity was set at 10 m/s. Each experimental cohort was subjected to a 6-minute aerodynamic erosion procedure, with resultant outcomes illustrated in Figure 11. From Figure 11, dust on the surface of the coal sample without dust suppression material quickly becomes airborne under airflow action. Particulate concentration peaked at 15.7 mg/m³ within 120 seconds, followed by asymptotic decay toward stabilization at approximately 11.4 mg/m³.Particulate generation persisted continuously. The Pure Water treatment group exhibited a certain dust suppression effect, while dust concentration decreasing to 8.5 mg/m³, then quickly dropping to an equilibrium concentration of about 2.1 mg/m³. Dust generation under wind flow disturbance lasted for 112 s, indicating that spraying pure water alone is difficult to effectively suppress dust. With incremental elevation of CBS-PAAS mass fraction from 0.5% to 2.0%, particulate peak concentration exhibited substantial reduction relative to aqueous control conditions. The corresponding asymptotic concentrations were determined to be 1.5 mg/m³, 1.5 mg/m³, 1.0 mg/m³, and 1.2 mg/m³, respectively. The temporal duration of particulate generation induced by aerodynamic perturbation was measured at 35 s, 90 s, 46 s, and 51 s, respectively.Observation indicates that CBS-PAAS mass fractions of 1.5% and 2.0% yield peak particulate concentrations below 3.5 mg/m³, with asymptotic stabilization values beneath 1.5 mg/m³.Furthermore, the temporal interval of particulate generation resulting from aerodynamic perturbation remained below 60 seconds.

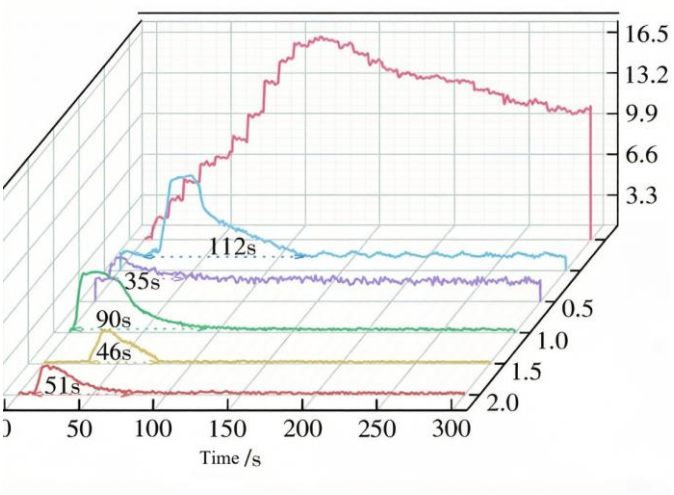


**Figure 11** Wind erosion experiment results

Cost-benefit analysis demonstrates that CBS-PAAS formulations with mass fractions of 1.5% and 2% incur costs of 0.23 × $10^4$ CNY/t and 0.3 × $10^4$ CNY/t, respectively, which are lower than commercially available common dust suppression materials (1.3 × $10^4$ ~ 1.8 × $10^4$ CNY/t).Under equivalent operational conditions, utilizing CBS-PAAS at 1.5% mass fraction versus 2% formulation yields a dust suppression cost reduction of approximately 0.5 × $10^4$ CNY per Coal Transportation Operation. Unlike conventional approaches, the present work leverages the inherent cellulose framework and porous architecture of corncob-derived bio-based materials to establish an interconnected network structure, thereby eliminating the risk of secondary contamination typically associated with synthetic chemical agents. Directionally arranged amphiphilic moieties within the three-dimensional porous framework enable superior moisture retention, eliminating the need for frequent water replenishment required by conventional wetting-based dust suppression agents.

The cellulose framework reinforces structural integrity and mechanical resilience, enabling effective particulate

binding and consolidation to satisfy the demanding requirements of vibrational stress environments characteristic of coal logistics operations. Subsequent investigations may delve deeper into elucidating how distinct physicochemical attributes of coal particulates—including mineral residue composition, surface electrokinetic potential, and liquid affinity—modulate the efficacy of the CBS-PAAS formulation. The incorporation of surface-active agents or chemical functionalization of the corncob substrate enables enhanced adaptability across diverse coal dust characteristics. Furthermore, developing an optimized proportioning framework would facilitate broader implementation of this biomaterial in practical applications.

**7 Conclusion**

(1) The ideal formulation is attained when acrylic acid, ethylene glycol dimethacrylate, and sodium dodecyl sulfate are combined in a 2:2:1 volumetric proportion, yielding the synthesis of corncob-derived polymeric dust suppressant (CBS-PAAS) possessing the desired architecture. This composite displays an interconnected framework, with its exterior featuring rapidly solubilizing, highly adsorptive lamellar morphologies.

A compact, lamellar solidified stratum develops atop the coal particulate surface, effectively occupying the interstitial voids among the coal particles.

(2) Computational investigations employing Materials Studio were conducted in this study to elucidate the microscale particulate mitigation mechanisms governing the suppressant's efficacy.Throughout the moistening phase, suppressant molecules exhibit oriented assembly toward the coal substrate terminus, generating an interconnected reticular architecture. Upon attaining diffusive equilibrium, the lipophilic moieties of the suppressant establish chemisorptive bonding with surface functionalities present on the coal, whereas the hydrophilic segments orchestrate aqueous infiltration into the coal matrix, thereby amplifying intermolecular engagement at the coal-water interface.(3) This paper constructed a simulation experimental system and verified the effectiveness of CBS-PAAS through experiments. At a 1.5% spraying mass fraction of CBS-PAAS, the maximum particulate concentration reached 3.0 mg/m³, with a steady-state concentration of 1.0 mg/m³ and a dust emission duration of 46 seconds under aerodynamic perturbation, demonstrating superior overall particulate suppression performance.

## References

[1] FAN Weicheng, MIAO Hongyan, YUAN Liang, et al. Development strategy of safety discipline in China during the 14th Five-Year Plan period[J]. Bulletin of National Natural Science Foundation of China, 2021, 35(6): 864-870.

[2] ZHOU Fubao, YUAN Liang, CHENG Weimin, et al. Research progress on occupational health protection technology of mine dust from 2013 to 2023[J]. Journal of Safety Science and Technology, 2023, 19(12): 5-15.

[3] WANG Boying. Study on coal railway transportation path and capacity expansion scheme from Xinjiang to Ningxia[J]. Journal of Railway Engineering Society, 2024, 41(8): 17-22.

[4] CHENG Weimin, ZHOU Gang, CHEN Lianjun, et al. Research progress and prospect of dust control theory and technology in China's coal mines in the past 20 years[J]. Coal Science and Technology, 2020, 48(2): 1-20.

[5] YAO Haifei, WANG Haiyan, LI Yanchuan, et al. Three-dimensional spatial and temporal distributions of dust in roadway tunneling[J]. International Journal of Coal Science & Technology, 2020, 7(1): 88-96.

[6] ZHANG Qingtao, ZHOU Gang, HU Yingying, et al. Microwetting dynamic behavior and mechanism for coal dust based on low field NMR method-A case study[J]. Fuel, 2021, 297: 120702.

[7] CHENG Shuyan, HAO Yanhong, XIN Yunling, et al. Synthesis of coal dust depressor by waste paper and its application[J]. Chinese Journal of Environmental Engineering, 2013, 7(9): 3578-3582. (in Chinese)

[8] LUO Ruidong, LIN Musong, LUO Yunbai, et al. Preparation and properties of a new type of coal dust suppressant[J]. Journal of China Coal Society, 2016, 41(S2): 454-459. (in Chinese)

[9] MA Yunlong, ZHOU Gang, LI Shuailong, et al. Synthesis and properties of a conglomeration-wetting spray agent for dust suppression[J]. Industrial & Engineering Chemistry Research, 2018, 57(42): 13940-13951.

[10] NIE Wen, XU Changwei, PENG Huitian, et al. Development and research on dust suppression performance

of a new type of spray dust suppressant for increasing moisturizing and accelerating coagulation in mines[J]. Materials Reports, 2023, 37(15): 264-272. (in Chinese)

[11] XU Changwei, NIE Wen, PENG Huitian, et al. Numerical simulation of the effect of a wind-assisted spraying device during continuous mining[J]. Powder Technology, 2023, 428: 118803.

[12] ZHOU Gang, LI Shuailong, XU Yixin, et al. Preparation and effect analysis of cedar sawdust-based super absorbent dust suppressant material[J]. Coal Science and Technology, 2023, 51(2): 232-242. (in Chinese)

[13] ZHOU Gang, ZHANG Xinyuan, LI Shuailong, et al. New type of sawdust-based dust suppressant during tunnelling and underground space: Preparation, characterization and engineering application[J]. Construction and Building Materials, 2023, 365: 130085.

[14] LI Yutong, KONG Yu, GUAN Lin, et al. Study on adsorption of phosphorus and hydrochloric acid by the combination of modified corncob biochar and steel slag micropowder[J]. Applied Chemical Industry, 2024, 53(8): 1761-1764. (in Chinese)

[15] WANG Liqiong, LI Xia, HOU Lin, et al. Adsorption properties of corncob and cyclodextrin crosslinked composites for dye molecules[J]. Applied Chemical Industry, 2024, 53(1): 10-14. (in Chinese)

[16] JIANG Dawei, WANG Ying, LI Bin, et al. Environmentally friendly alternative to polyester polyol by corn straw on preparation of rigid polyurethane composite[J]. Composites Communications, 2020, 17: 109-114.

[17] MOHITE Aishwarya S, JAGTAP Ameya R, AVHAD Madhavi S, et al. Recycling of major agriculture crop residues and its application in polymer industry: A review in the context of waste to energy nexus[J]. Energy Nexus, 2022, 7: 100134.

[18] ZHU Shiliu, GUO Yong, TU Daowu, et al. Water absorption, mechanical, and crystallization properties of high-density polyethylene filled with corncob powder[J]. BioResources, 2018, 13(2): 3778-3792.

[19] JIN Shuping, CHEN Jun, MAO Jianying, et al. A novel superabsorbent from raw corn straw and poly(acrylic acid)[J]. Polymer Composites, 2017, 38(7): 1353-1362.

[20] WANG Weishuai, YANG Shiqi, ZHANG Aiping, et al. Preparation and properties of novel corn straw cellulose-based superabsorbent with water-retaining and slow-release functions[J]. Journal of Applied Polymer Science, 2020, 137(32): 48951.

[21] YANG Jiatian, TANG Jinming, LIANG Zirong, et al. Preparation and application of novel starch-based super absorbent polymer dust suppressant[J]. Chemical Industry and Engineering Progress, 2023, 42(6): 3187-3196. (in Chinese)

[22] WANG Kai, XU Min, YANG Mengjiao, et al. Study on mechanism of coal dust wettability influenced by multiple factors[J]. Journal of Safety Science and Technology, 2023, 19(11): 78-85. (in Chinese)

[23] ZHOU Gang, XU Yixin, WANG Yongmei, et al. Study on MICP dust suppression technology in open pit coal mine: Preparation and mechanism of microbial dust suppression material[J]. Journal of Environmental Management, 2023, 343: 118181.

[24] QIN Jianping, LI Beibei, YANG Tao, et al. Application of test method for dust suppression efficiency of wind erosion dust suppressant[J]. Environmental Science, 2019, 40(9): 3935-3941. (in Chinese)

[25] ZHANG Zhijun, WANG Lu, LI Hao. Study on model construction and optimization of molecular structure[J]. Coal Science and Technology, 2021, 49(2): 245-253. (in Chinese)

[26] XU Rongxiao, YU Haiming, DONG Hui, et al. Preparation and properties of modified starch-based low viscosity and high consolidation foam dust suppressant[J]. Journal of Hazardous Materials, 2023, 452: 131238.

[27] DONG Hui, YU Haiming, XU Rongxiao, et al. Application and characterization of new polymer dust suppression foam in coal mine and tunnel construction space[J]. Construction and Building Materials, 2023, 397: 132378.

[28] ZHOU Gang, LIU Yongwei, LI Shuailong, et al. Effects of SDBS and BS-12 on functional groups/wettability of multicomponent acidified lignite[J]. Journal of Molecular Liquids, 2023, 390: 122908.